ORIGINAL ARTICLE

# Efficient adsorption of Sudan dyes from food and plants by activated carbon derived from Nelumbinis stamen

Ya-Ling Yu[1] · Jun Cao[1]

## Abstract

This study uses phosphoric acid activation and carbonization processes to create Nelumbinis stamen activated carbon (NSAC) from food waste precursors in a single step. The resultant NSAC was characterized by scanning electron microscopy, Fourier transform infrared spectroscopy, $N_2$ adsorption/desorption methods, X-ray diffraction, and Raman spectroscopy for surface morphology, structural features, and surface chemistry. The operating conditions, including the carbonization temperature, amount of adsorbent, adsorption temperature, and aqueous solution pH, were optimized to maximize the removal efficiency of Sudan dyes. Therefore, the values of the optimized conditions were selected as 500℃ for the carbonization temperature, 0.4 g L$^{-1}$ for the adsorbent dose, 50℃ for the adsorption temperature, and a pH of 3.0 for the aqueous solution. In addition, the pseudosecond-order kinetic model and Langmuir isotherm model fit the experimental data best. Moreover, the maximum adsorption capacities of the four dyes on NSAC calculated according to the Langmuir adsorption model were in the range of 34.60–38.97 mg g$^{-1}$. Furthermore, thermodynamic results revealed that the adsorption process was spontaneous, feasible, and endothermic. Finally, the activated carbon was used for the adsorption of Sudan dye solution from chrysanthemum tea and cooked egg samples, and the results showed that the adsorbent could be successfully used for the adsorption and removal of the dyestuff solution.

**Keywords** Activated carbon · Adsorption · Food waste · Nelumbinis stamen · Sudan dyes

## 1 Introduction

With the rapid growth of the global economy, the demand and scale of the food industry continue to rise, resulting in an increasing amount of food waste in both developing and developed countries as an important component of municipal solid waste (MSW). According to a recent study by the Food and Agriculture Organization of the United Nations (FAO), approximately 1.6 billion tons of food waste is generated worldwide each year during the production or consumption process [1]. Therefore, proper and safe disposal of food waste has attracted widespread attention from the public. Traditional methods of disposal of food waste include incineration, composting, animal feeding, or landfilling [2, 3]. However, due to the rich organic matter in food waste, improper disposal induces rot, odor, and virus infection, thereby polluting surface water, the surrounding atmosphere, and the environment [4, 5]. At present, the conversion of food waste into value-added products has received great attention, and some industries are emerging, such as bioactive compound extraction, biogas, biofuel production, bioplastic synthesis, and activated carbon synthesis [6]. Among these new technologies, activated carbon is obtained by pyrolysis and carbonization of food waste, which is not only low in cost but also in line with the concept of green chemistry. In the reported papers, food waste activated carbon, including banana peels [7], tangerine seed [8], hawthorn kernel [9], coffee waste [10], pecan nutshell, and para chestnut husk [11], has been studied for its promising adsorption efficiency for the removal of pollutants.

Activated carbon is the carbonaceous material that is produced from biomass as raw material under certain pyrolysis temperatures [12]. There are two ways to transform biomass into activated carbon: (a) chemical activation and (b) physical activation. Physical activation is carried out as a two-step process: the raw materials are pyrolyzed and converted into activated carbon under an inert atmosphere, and then

✉ Jun Cao
caoj@hznu.edu.cn; caojun91@163.com

1 College of Material Chemistry and Chemical Engineering, Hangzhou Normal University, Hangzhou 311121, China

the activated carbon derived from pyrolysis is activated. Chemical activation is a single step, where the pyrolysis and activation processes are carried out at the same time. Generally, chemical activation is performed at a low working temperature with simple operation, and the obtained activated carbon has a higher surface area and larger pore volume. As one of the most important activators in activated carbon preparation, $H_3PO_4$ is able to hydrolyze cellulose at lower temperatures by breaking the bonds that produce long cellulose chains, thus breaking down lignocellulosic precursors. The high acidity of $H_3PO_4$ (pKa = 2.16) makes it an effective and environmentally friendly activator for hydrolysis, dehydration, destruction of the biomass skeleton and formation of pores [13, 14]. Because of its excellent physical and chemical properties, such as large surface area, porous structure, thermal stability, and multiple functional groups in the chemical structure, activated carbon could be used to improve the quality of the ecological environment in a variety of agricultural, biorefinery, and environmental fields [15]. The adsorption and removal of heavy metals and organic pollutants is an important capacity of activated carbon. Various pollutants to be removed from effluents by activated carbon have been studied, such as pharmaceutical compounds [16], pesticides [17], heavy metals [18, 19], and dyes [20].

Sudan dye is a class of synthetic azo dyes with benzozophenol as the main group, is generally insoluble in water and soluble in organic solvents, and is widely used in the dyeing of industrial products. For example, these dyes are used as color enhancers in waxes, shoes, clothing, and cosmetics [21]. However, Sudan dyes can cause irreversible harm to the human body if consumed. Because of its strong lipophilicity, Sudan dye, once in the human body, cannot be excreted through urine, and its azo group-released aniline can cause liver disease while being metabolized, even leading to cancer due to genetic mutations [22]. Unfortunately, due to the bright color and low price of Sudan dyes, they are often illegally added to various foods, such as tomato paste, paprika, and foods containing chili peppers [23, 24]. Additionally, there are also cases in industrial production where Sudan dyes are mishandled and become potential sources of environmental pollution, threatening human health and the safety of ecosystems. At present, there are many detection and extraction techniques for Sudan dyes, such as high-performance liquid chromatography−mass spectrometry (HPLC−MS) and micellar electrokinetic chromatography-MS/MS in detection methods and deep eutectic solvent-assisted solid-phase extraction methods in extraction methods [21, 24, 25]. Interestingly, there are few reports on methods for removing Sudan dyes from a complex sample matrix, so developing an environmentally friendly and inexpensive adsorbent for the removal of Sudan dyes is a promising study.

Nelumbinis stamens are the dried stamens of lotus plants, of which flavonoids are the main characteristic chemical components that have the effect of clearing the heart, benefiting the kidneys, and stopping bleeding [26]. As a medicinal and food plant, lotus is widely cultivated and used in China and other countries. However, the medicinal value of the traditional medicine of Nelumbinis stamens has not yet attracted attention, resulting in the abandonment of Nelumbinis stamens. The filament and pollen structure of the Nelumbinis stamens make them both rich in fiber structure and high phospholipid content pollen, they have great potential as precursors of phosphorus-doped activated carbon materials [27]. However, there has been no report on the application of Nelumbinis stamens to make activated charcoal. Therefore, the use of Nelumbinis stamen as a precursor material along with phosphoric acid activation and a single-step carbon production method to produce Nelumbinis stamen activated carbon (NSAC) is intriguing.

In this study, NSAC was prepared for the first time from food waste precursors using a single-step method that included phosphoric acid activation and carbonization. The structural characterization of the synthesized activated carbon was carried out by scanning electron microscopy, infrared spectroscopy, and X-ray diffraction, and adsorption conditions such as charring pyrolysis temperature, adsorbent dosage, adsorption temperature, and solution pH were optimized. Finally, the activated carbon was used for the adsorption of Sudan dye solution based on chrysanthemum tea and cooked egg samples, and the results showed that the adsorbent could be successfully used for the adsorption and removal of the dyestuff solution.

## 2 Materials and methods

### 2.1 Chemicals and reagents

Sudan Red G, Sudan I, Sudan II, and Sudan Red 7B were obtained from Merck KGaA (Darmstadt, Germany) with purities in the range of 98–99%. The chemical specifications of the Sudan dyes are listed in Table S1. Analytical-grade hydrochloric acid was provided by Sinopharm Chemical Reagent Co., Ltd. (Shanghai, China). Analytical-grade sodium hydroxide was purchased from Alfa Aesar China (Tianjin, China). Purified water was purchased from Wahaha Group, Ltd. (Hangzhou, China) during the study. HPLC-grade acetonitrile and methanol were obtained from Tedia Company Inc. (Fairfield, US). HPLC-grade water was supplied by J.T. Baker (Deventer, the Netherlands). The Nelumbinis stamen sample was purchased from Hangzhou, Zhejiang Province, and produced in Xiangyang, Hubei Province. Chrysanthemums tea and cooked egg samples were obtained from a local supermarket (Hangzhou, China).

## 2.2 Analytical conditions

Four dyestuffs under investigation were analyzed by an Agilent 1290 series HPLC system (Agilent Technologies, Inc., USA) connected with an autosampler and ultraviolet detector (UV). An Agilent Poroshell 120 EC-C18 column (4.6 mm × 100 mm, 2.7 μm Agilent Technologies Inc., USA) was employed for HPLC analysis. The flow rate of the mobile phase, injection volume, and column temperature were set at 0.4 mL min$^{-1}$, 2 μL, and 30 °C, respectively. The UV detection wavelength was set at 520 nm. The mobile phase was water (A) and methanol (B), and the optimized gradient program was as follows: 0 min, 40% B; 0–2 min, 40%-100% B; 4–13 min, 100%-100% B; 13–15 min, 100%-40% B.

## 2.3 Sample treatment

Standard stock solutions of Sudan Red G, Sudan I, Sudan II, and Sudan Red 7B were prepared by mixing each analyte in acetonitrile (1 mg mL$^{-1}$) and kept at 2–4℃. The standard solutions used during the experiment were obtained by dilution of each stock solution with water to different concentrations. Additionally, the resulting solution was centrifuged at 13,000 rpm for 5 min, and the supernatant was used for the analysis.

To verify the effectiveness of the adsorption method, chrysanthemum and cooked egg samples were analyzed. The sample preparation process was as follows. One gram of accurately weighed chrysanthemums was soaked in hot water at 80 °C for 20 min, and the supernatant was collected for the adsorption experiments after cooling. The egg sample was obtained by mashing the cooked egg, and then 5 g of egg yolk was ultrasonically extracted with 20 mL of 60% acetonitrile for 30 min. The supernatant was centrifuged at high speed at 15,000 rpm for 3 min and filtered for later use.

## 2.4 Adsorbent preparation

Nelumbinis stamen samples bought in the local market were dried in an oven at 60 °C for 6 h, crushed and passed through a 60-mesh sieve plate. Next, Nelumbinis stamen powder was transferred to 60 wt% H$_3$PO$_4$ at a ratio of 1:5 (W/V) at room temperature for 2 h. The activated powder was then left in a drying cabinet to evaporate water at 65 °C overnight. The carbonization process of converting the powder to carbon was as follows. The carbonization temperature was heated from room temperature to the final temperature at a heating rate of 10 K min$^{-1}$ and kept for 3 h. Afterward, the material obtained after cooling was washed with distilled water until the pH value was approximately 6–7. Finally, the NSAC was dried overnight at 60 °C in an oven. The adsorbent preparation steps are summarized in Fig. S1.

## 2.5 Characterization studies

The surface functional chemistry of the raw material and activated carbon were analyzed using a Fourier Transform Infrared Spectrometer (FTIR, Bruker vertex 70 V, Germany) with wavelengths between 400 and 4000 cm$^{-1}$. Scanning electron microscopy (SEM, Hitachi TM3000, Japan) was used to scrutinize the surface microstructures of the activated carbons. The specific surface area of NSAC samples was accurately quantified in a N$_2$ atmosphere maintained at an operating temperature of 77 K under a relative pressure (p/p$_0$) of 0.40–0.90 by the Brunauer–Emmett–Teller (BET) method. The BET method was used to determine the pore size and volume of the sample using standard physisorption equipment (Quantachrome, American). The sample pore size and pore volume were evaluated using the Barrett–Joyner–Halenda (BJH) formula. Raman spectroscopy of NSAC was obtained with the help of a confocal Raman microscope (Renishaw inVia Laser Raman Microscope, UK). The XRD patterns of NSAC were collected on an X-ray diffractometer (XRD, Bruker D8 Advance, Germany).

## 2.6 Adsorption performances

Adsorption experiments to obtain the optimal conditions were performed with 2 mg of NSAC and 10 mL of Sudan Red G, Sudan I, Sudan II and Sudan Red 7B solution in 50 mL glass bottles, which were fixed to a magnetic stirrer and stirred at a constant rate of 250 rpm for 20 min. The adsorption effect of activated carbon under different carbonization temperatures (400, 450, 500, 550, and 600℃) was investigated to determine the optimum carbonization temperature. The adsorption performance of the NSAC was also studied by adding different amounts (1, 2, 4, 6, and 8 mg) of activated carbon to 10 mL of dye solution at different adsorption temperatures (20, 30, 40, 50, and 60℃) or pH values (3, 5, 6, 9, and 10). The kinetic experiment was performed by filling a series of Erlenmeyer flasks with 10 mL dye solutions of different concentrations (5–15 mg mL$^{-1}$). After mixing and stirring for a predetermined time (1 to 17 min), the solution was withdrawn from the sample mixture, centrifuged, and tested by HPLC to investigate the effect of different initial concentrations and contact times on adsorption. Finally, an isotherm study was performed, and for this step, equilibrium curves were obtained at temperatures between 30 and 50℃ in dye solutions ranging from 5 mg mL$^{-1}$ to 15 mg mL$^{-1}$.

$$\text{Removal\%} = \frac{C_i - C_e}{C_i} \times 100 \tag{1}$$

$$qt = \frac{(C_i - C_t)V}{W} \tag{2}$$

$$qe = \frac{(C_i - C_e)V}{W} \tag{3}$$

where $C_i$ is the initial dye solution concentration (mg L$^{-1}$), $C_e$ denotes the equilibrium dye concentration (mg L$^{-1}$), $C_t$ depicts the dye concentration after certain minutes t being absorbed by NSAC (mg L$^{-1}$), V represents the volume of dye solution (mL) and W is the weight of NSAC (mg).

## 2.7 Adsorbent regeneration

To investigate the feasibility of reusing activated carbon, the adsorbent was desorbed from the adsorbent by stirring and a chemical eluent. The NSAC adsorbed with Sudan dye was collected and stirred with ethanol as the elution agent at 400 rpm for 6 h at room temperature. The desorbed NSAC was cleaned with distilled water, filtered and dried as the adsorbent for the next cycle. Three cycles were repeated to verify the regeneration of the NSAC.

## 3 Results and discussion

### 3.1 Optimal conditions for preparing NSAC

In the preparation process of activated carbon, the carbonization temperature has a significant effect on the yield of activated carbon, the specific surface area and the formation of surface functional groups. With the increase in the carbonization temperature and the extension of the carbonization time, the volatile components in the sample are pyrolyzed, and a large amount of organic matter, including cellulose and lignin, is decomposed, which causes a great loss of sample weight. To study the effect of carbonization temperature on the adsorption efficiency, five different temperatures (400, 450, 500, 550, and 600℃) were investigated, and the results are displayed in Fig. 1. As the carbonization temperature increased from 400 to 500℃, the removal efficiency was found to be improved and showed the best adsorption effect at 500℃. However, the adsorption effect was found to decrease with a further increase in carbonization temperature. The reason for this could be that as the carbonization temperature increased, new micropores were continuously formed inside the activated carbon, which made its specific surface area continuously increase, thereby improving the adsorption effect of the dye. However, when the temperature was further raised, part of the microporous structure was destroyed due to the excessively high temperature of the activated carbon, resulting in a decrease in the adsorption effect of the activated carbon. In addition, a higher carbonization temperature could speed up the carbonization reaction rate, and more carbon will be pyrolyzed, resulting in a low yield
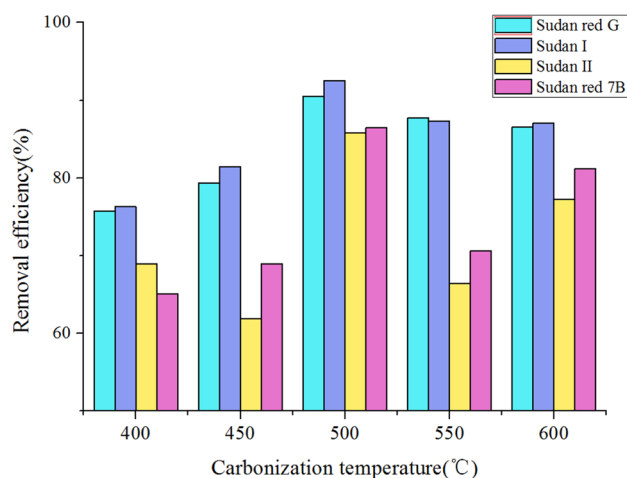


**Fig. 1** The effect of carbonization temperature on the adsorption efficiency. Five temperatures: 400℃, 450℃, 500℃, 550℃, 600℃

of activated carbon. Thus, the carbonization temperature of 500℃ was selected as the optimal temperature.

### 3.2 Characteristics of NSAC

The surface morphologies of raw Lotus stamen material and the prepared NSAC are shown in SEM images (Supplementary materials). The raw Lotus stamen sample (Fig. S2a, b) showed a compact surface with irregular particle shapes and no obvious crack distribution. The NSAC sample (Fig. S2c, d) exhibited a rough surface with new pores of irregular and randomly distributed sizes. These results indicated that the carbonization process led to visible changes in the increase of NSAC surface pores, and the openings and gaps of various sizes scattered on the surface could increase the contact area, which was beneficial to the adsorption process of pesticides. In addition, the improvement of the adsorption effect was also related to the role of H$_3$PO$_4$ in the hole-drilling effect that regulates the development of mesopores in the carbon matrix.

According to the International Union of Pure and Applied Chemistry (IUPAC) classification, the material nitrogen adsorption/desorption isotherms were considered to be type IV, consistent with H4 hysteresis loop characteristics (Fig. 2a) [28]. When the relative pressure (p/p$_0$) was 0.40–0.90, the curve showed mesoporous adsorption, and when p/p$_0$ was greater than 0.90, the curve was related to multilayer adsorption through macropores. The adsorption of these isotherms decreased at higher relative pressures (p/p$_0$), indicating that the adsorbent possessed a combination of micropores and mesopores. Moreover, the H4 hysteresis loop is common in adsorbents filled with mesopores and micropores, and the phenomenon was due to the capillary condensation effect. The total pore volume and BET specific

**Fig. 2** N$_2$ adsorption/desorption isotherms (**a**) and the average pore diameter of the NSAC (**b**)
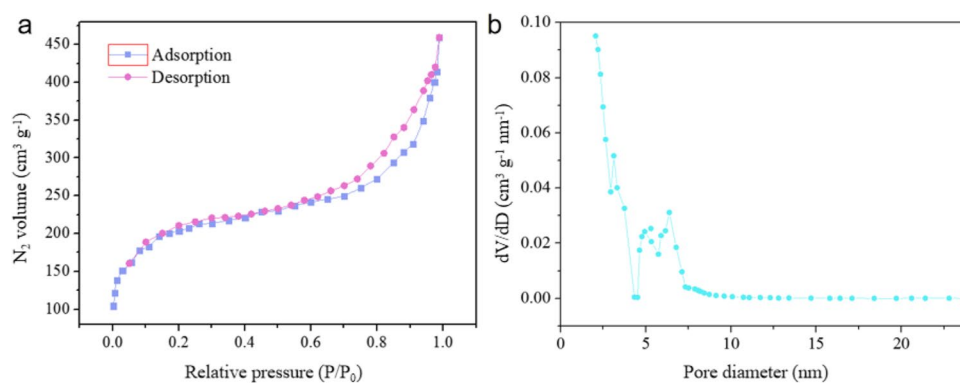


surface area of the NSAC were 0.509 cm$^3$ g$^{-1}$ and 732.98 m$^2$ g$^{-1}$, respectively. Figure 2b illustrates that the average pore diameter of the NSAC was distributed at approximately 2.03 nm, conforming to the results of nitrogen adsorption–desorption isotherms that the pores of the NSAC were abundant micropores and mesopores.

The FTIR spectra for both the precursor material (Nelumbinis stamen) and the activated carbon NSAC are displayed in Fig. 3a. Their corresponding peaks were observed at 3442 cm$^{-1}$ and 1632 cm$^{-1}$, which were related to typical O–H stretching vibrations in the hydroxyl functional groups and the overlaps of C＝O stretching vibrations with O–H bending variations. Starting with the Nelumbinis stamen, the peak at 2845 cm$^{-1}$ along with 2928 cm$^{-1}$ corresponds to asymmetric or symmetric vibrations of the C-H bond in the -CH2- group. In addition, the peaks at approximately 1748 cm$^{-1}$, 1400 cm$^{-1}$, and 1250 cm$^{-1}$ indicated C＝O stretching vibration, -CH3 bending vibration, and C-O bending vibration, respectively. After carbonization, the peaks of NSAC 2928 cm$^{-1}$, 2845 cm$^{-1}$, 1400 cm$^{-1}$, and 1250 cm$^{-1}$ disappeared, which could be related to the breaking of chemical bonds in organic compounds during the carbonization process. The presence of C＝O, C-O, C＝C, C-H, and O–H bonds can confirm the presence of methyl, carbonyl, and hydroxyl structures on the NSAC surface, which might affect the adsorption of dyes on NSAC activated carbon.

In the XRD pattern of NSAC (Fig. 3b), two broad peaks are found at 23.57 and 42.46, and each corresponding to

**Fig. 3** Characteristics of NSAC. **a**: Infrared spectrum; **b**: XRD pattern; **c**: Raman spectrum
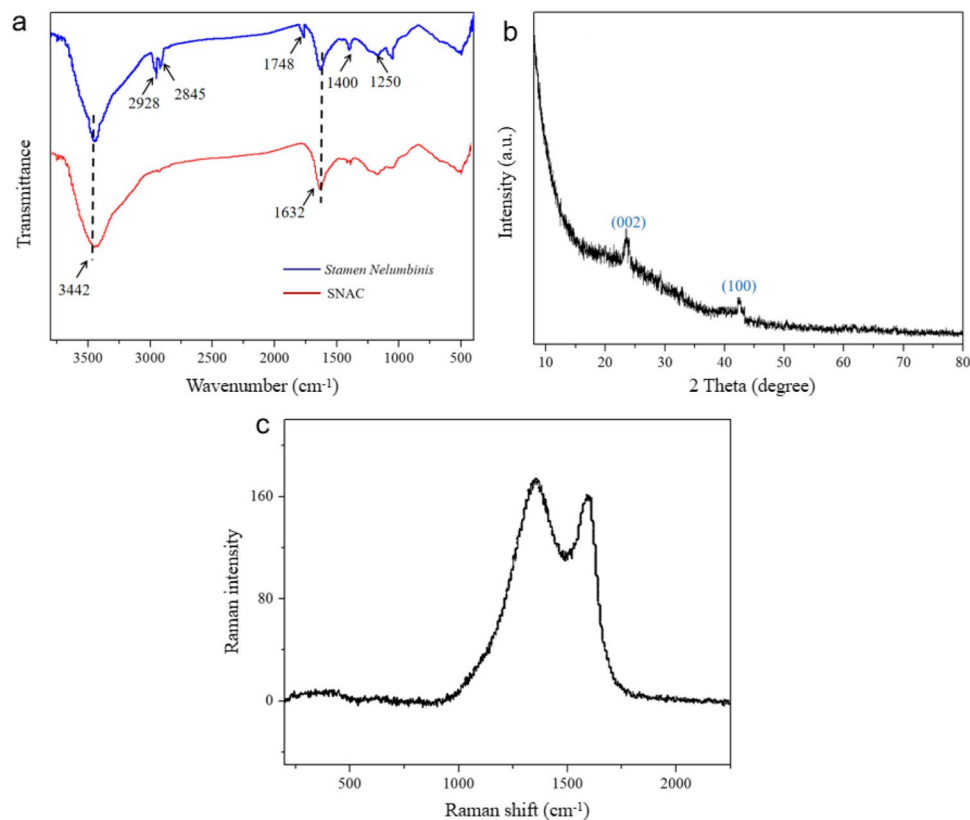
the (002) plane and (100) plane, indicating that the synthesized carbon was amorphous in nature [29]. In the Raman spectrum (Fig. 3c), two distinct broad peaks, including the D-band (1354 cm$^{-1}$) and G-band (1589 cm$^{-1}$), were ascribed to sp$^3$ hybridized carbon with a disordered state and sp$^2$ hybridized carbon with an ordered structure, respectively. The intensity ratio of the D-band to the G-band ($I_D/I_G$) was 1.08, which was consistent with the amorphous structure in the XRD results that the defects in the compound were due to the SP$^2$ carbon network and the C=C bond or aromatic carbon [30].

### 3.3 Optimal conditions for adsorbing dye solution

To obtain the optimal adsorption conditions, the adsorbent dosage must be determined. The effect of adsorbent dosage on removal efficiency was studied using active carbon in five different amounts ranging from 0.1 to 0.8 g L$^{-1}$, each in a 10 mL dye solution with a concentration of 10 g mL$^{-1}$. The effect of the adsorbent dose on the removal efficiency percentage of the dye solution is shown in Fig. 4a. The results

indicated that the adsorption efficiency of NSAC increased from 67.87% to 92.13% for Sudan red G, from 69.24% to 95.57% for Sudan I, from 78.91% to 90.06% for Sudan II, and from 76.54% to 91.75% for Sudan red 7B with increasing doses from 0.1 to 0.4 g L$^{-1}$. This should be attributed to the fact that the gradual increase in the dose of adsorbent, as predicted by many documents, could increase the availability of active sites due to the high surface area, resulting in an increase in the adsorption removal efficiency. Nevertheless, an adsorbent value higher than 0.4 g L$^{-1}$ had little effect on dye adsorption. Furthermore, an excessive amount of adsorbent might cause the aggregation of particles and result in a decrease in the adsorption capacity of the adsorbent. Based on the above experiments, 0.4 g L$^{-1}$ was selected as the optimal dose of NSAC, achieving an average removal efficiency of 92.42% for the four dyes.

Adsorption temperature has an effect on the chemical structure of the activated carbon surface and the activity of functional groups. In addition, the change in the solution temperature could also affect the thermal movement of the analytes in the water. Under an initial dye concentration
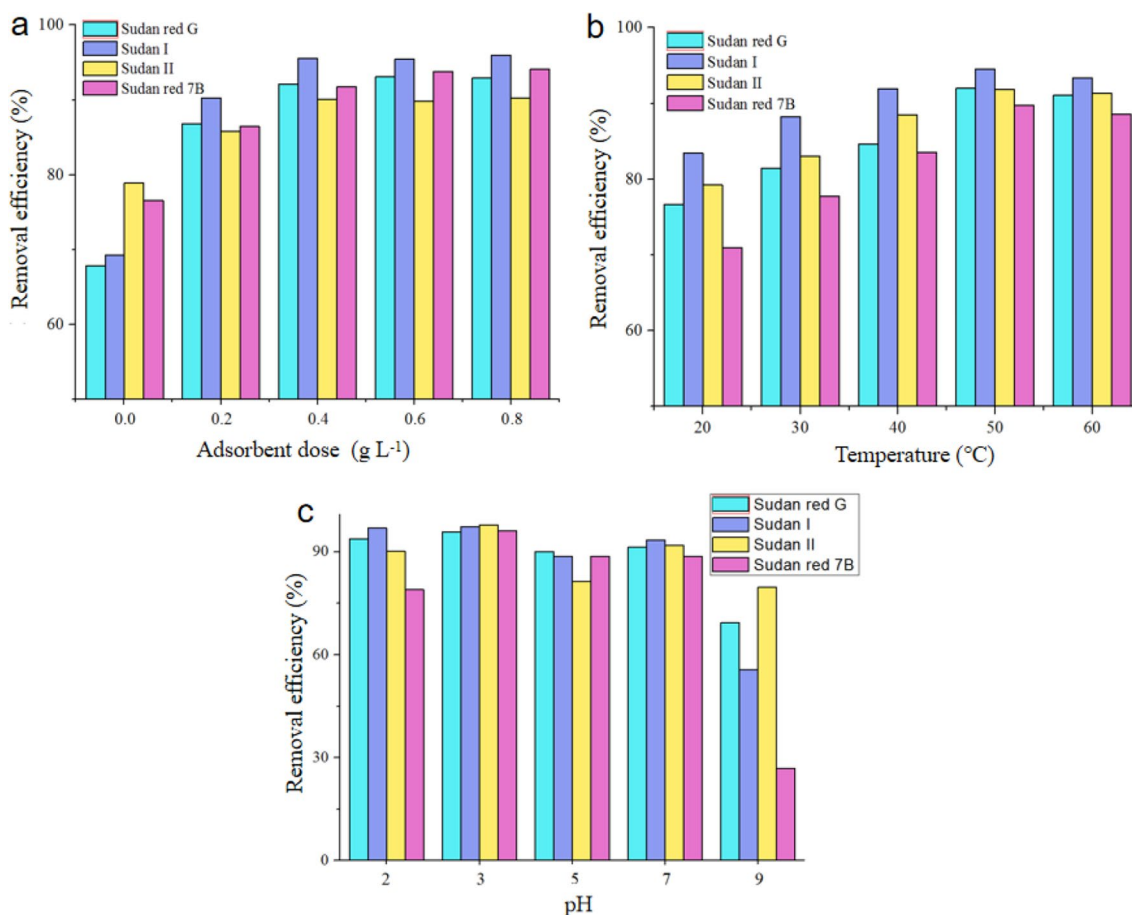


**Fig. 4** Effect of adsorption conditions on dye removal. a: adsorbent dose (0, 0.2, 0.4, 0.6, and 0.8 g L.$^{-1}$); b: adsorption temperature (20, 30, 40, 50, and 60℃); c: pH of the adsorption solution (2, 3, 5, 7, and 9)

of 10 µg L$^{-1}$ and original pH values, the effect of adsorption temperature was examined by using different adsorption temperatures (20, 30, 40, 50, and 60°C) and a constant NSAC amount (0.4 g L$^{-1}$). It can be seen in Fig. 4b shows that the adsorption efficiency increased as the temperature increased. When the temperature was raised to 50 °C, the increasing trend of the removal efficiency was basically stable. The results illustrated that the removal rate increased with increasing temperature, indicating that high temperature promotes the adsorption of NSAC with dyes and is an endothermic process, which is consistent with the endothermic conclusions obtained in thermodynamic studies. As a consequence, an adsorption temperature of 50 °C was chosen for further experiments.

The change in the pH value of the solution could affect the existing state of the molecule and the existing form of the surface charge of the biomass carbon, which is an important factor affecting the adsorption effect. By using a constant initial dye concentration (10 µg mL$^{-1}$) and NSAC amount (0.4 g L$^{-1}$) at an adsorption temperature of 50 °C, the pH impact was investigated by taking various pH values from 2 to 9 (Fig. 4c). As the pH value increased from 2.0 to 9.0, the removal percentage of NSAC for dye adsorption decreased gradually in general and achieved a maximum pH of 3.0 (zeta potential -7.78 mV). The high dye removal efficiency % (88.6–97.84%) at low pH values could be explained by π-π interactions and hydrogen bonds between dyes and NSAC, and the presence of H$^+$ ions could promote the adsorption of dye solutions. However, when the pH of the solution was changed from neutral to alkaline, the removal percentage dropped sharply, which could be due to the binding of OH$^-$ ions with the cation charge sites of dye molecules, resulting in competition between the OH$^-$ ions and the active sites of biological carbon. As a consequence, the value of pH 3 was selected for use in further kinetics and isotherm experiments.

## 3.4 Adsorption kinetics of NSAC

A high adsorption rate in addition to a high adsorption capacity is a key parameter for evaluating adsorbents. To obtain detailed information about adsorption equilibrium time and adsorption effects, the contact time between adsorbents and adsorbents of different concentrations was studied. The variations in the adsorption capacity of NSAC adsorption at different initial dye concentrations of 5, 7.5, 10, 12.5, and 15 mg L$^{-1}$ were evaluated using adsorption capacities ($q_t$) as a function of contact time (t) varying from 0 to 16 min, and the results of Sudan Red G (a), Sudan I (b), Sudan II (c) and Sudan Red 7B (d) are illustrated in Fig. 5. For Sudan Red G, the process reached equilibrium after 16 min with capacities of 12.5, 18.11, 24.22, 30.1 and 34.57 mg g$^{-1}$, increasing with

concentration, and the other three analytes, Sudan I, Sudan II, and Sudan Red 7B, had similar kinetic behaviors. The higher initial concentration of the solution was accompanied by a higher equilibrium adsorption capacity, which could be attributed to the rapid transfer of dye molecules to the vacancies on the NSAC surface and the high driving force. In addition, the adsorption of dyes onto NSAC occurred rapidly, showing high $q_t$ values at relatively short times. This could be caused by the large surface area and abundant active sites of NSAC.

To study the kinetics of the adsorption process of the four dyes by NSAC and explain the adsorption rate and adsorption mechanism, three widely reported kinetic models, the pseudofirst-level model (Eq. (4)), the pseudosecond-level model (Eq. (5)) and intraparticle diffusion (Eq. (6)), were investigated using linear regression based on experimental data:

$$\log(q_e - q_t) = \log q_e - \frac{k_1 t}{2.303} \tag{4}$$

$$\frac{t}{q_t} = \frac{1}{k_2} q_e^2 + \frac{t}{q_e} \tag{5}$$

$$q_t = k_i t^{0.5} + C \tag{6}$$

where $q_e$ (mg g$^{-1}$) and $q_t$ (mg g$^{-1}$) are the amount of dyes adsorbed onto NSAC at equilibrium and a random time t (min), respectively. $k_1$ (min$^{-1}$) and $k_2$ (g mg$^{-1}$ min$^{-1}$) are the rate constants of the pseudofirst-order and pseudosecond-order models, respectively. C is the constant related to the thickness of the boundary layer, and $k_i$ is the intraparticle diffusion rate constant (mg g$^{-1}$·min$^{-0.5}$). The values of $k_1$ and $q_e$ could be estimated from the linear plot of log ($q_e$-$q_t$) versus t, respectively. The slope and the intercept obtained from the curve of t/$q_t$ against t allowed the calculation of $k_2$ and $q_e$, respectively. By plotting a curve of $q_t$ versus $t^{0.5}$, the values of $k_i$ and C could be calculated.

The pseudofirst-level and pseudosecond-level models' linear curves are illustrated in Fig. 6(a, b), respectively. The information about the model parameters of the kinetic equations and fitting coefficient of correlation $R^2$ were measured on the determination of the linear plot of models, and the results are displayed in Table 1. Obviously, the $q_e$ (cal) values obtained from the pseudosecond-order model were closer and identical to the experimental values $q_e$ (exp) for the dye adsorption test, which implied that the adsorption process could be controlled by chemical adsorption and involved electron transfer and sharing between the NSAC surface groups and the dye molecules [31]. In addition, compared to the value obtained using the pseudofirst-order model, this model showed a higher and closer $R^2$ value to 1. Therefore, the pseudosecond-order kinetic equation is the
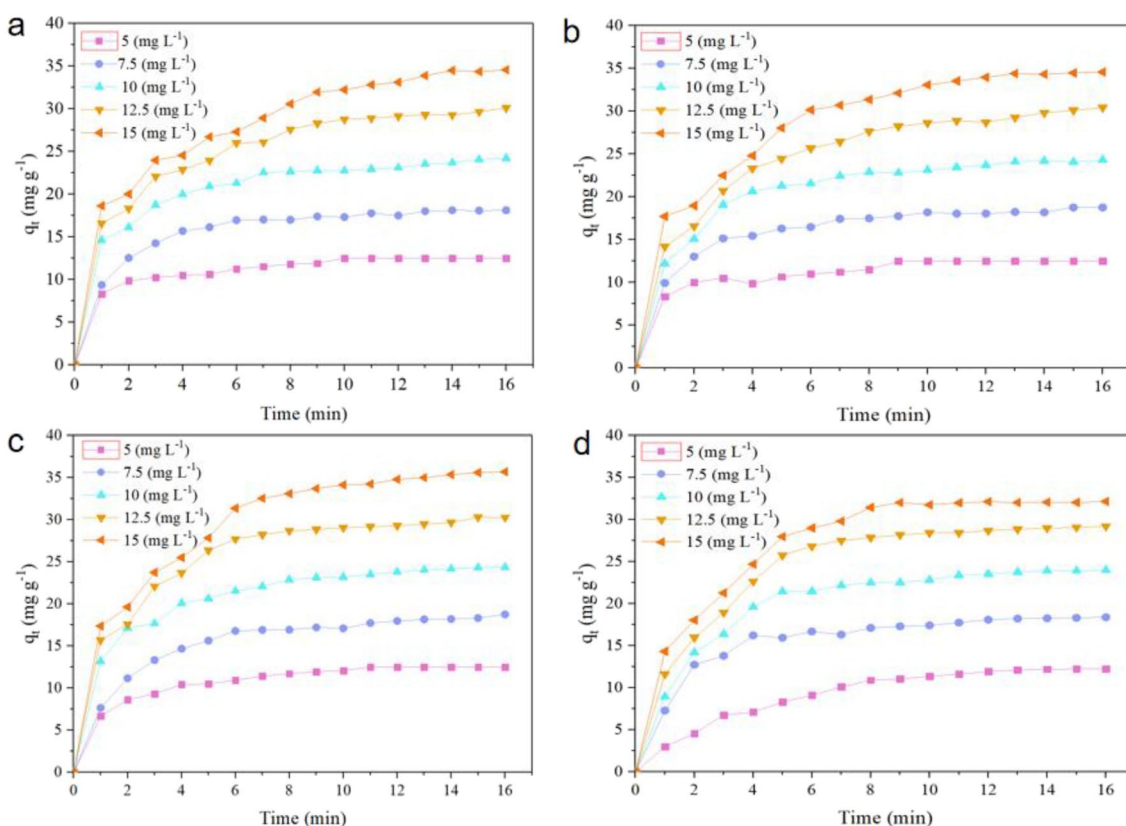
**Fig. 5** Effects of different adsorption times and initial concentrations on (**a**) Sudan Red G, (**b**) Sudan Red I, (**c**) Sudan Red II, and (**d**) Sudan Red 7B adsorbed on NSAC

best fitting kinetic model for describing the adsorption process between NSAC and dye solution.

For solid adsorbents with obvious pores on the material, NSAC is permeable to the dye molecules onto the surface, so the external mass transfer, intraparticle diffusion, and saturation still play an important role in the adsorption process. As shown in Fig. 6c and Table 2, the plot of qt versus $t^{1/2}$ was divided into two separate linear portions rather than one straight line, indicating that intraparticle diffusion is not the only rate-controlling step and that two or more factors affect the adsorption process. The steep slope observed in the first straight section indicated that the interparticle diffusion appeared as a rapid outer diffusion step. In addition, the first straight line did not pass through the origin with positive intercepts, showing that both interparticle diffusion and external mass transfer were involved in the adsorption of the dye solution. The second linear part indicates intraparticle diffusion (the dye diffusion within the pores of the NSAC) and adsorption equilibrium. When the dye molecules were transferred from the surface to the adsorbent pores, the diffusion resistance increased, so the diffusion speed decreased. With decreasing dye concentration, the diffusion rate decreased, and the diffusion process achieved the final equilibrium stage.

## 3.5 Adsorption isotherm studies of NSAC

To study the effects of temperature on the adsorption performance of dyes on NSAC, two commonly used isotherm models, Langmuir and Freundlich, are employed to describe how the adsorbed molecules interact with the adsorbent [32, 33]. The Langmuir isotherm model is one of the typical representatives of nonlinear adsorption theoretical treatment methods and is used to describe the phenomenon that the absorption process occurs on a completely uniform and uniform energy surface through monolayer adsorption, and there is no interaction between adsorbed molecules. The Langmuir isotherm model can be presented as Eq. (7). The Freundlich isotherm is a nonlinear adsorption theoretical model that is utilized to confirm the adsorption strength of the adsorbent surface with an incomplete energy distribution and proposes a multilayer adsorption mechanism accompanied by the interaction between adsorbed molecules. The common formula of this model is given in Eq. (8).

$$\frac{1}{q_e} = \left(\frac{1}{K_L q_{max}}\right)\frac{1}{C_e} + \frac{1}{q_{max}} \tag{7}$$

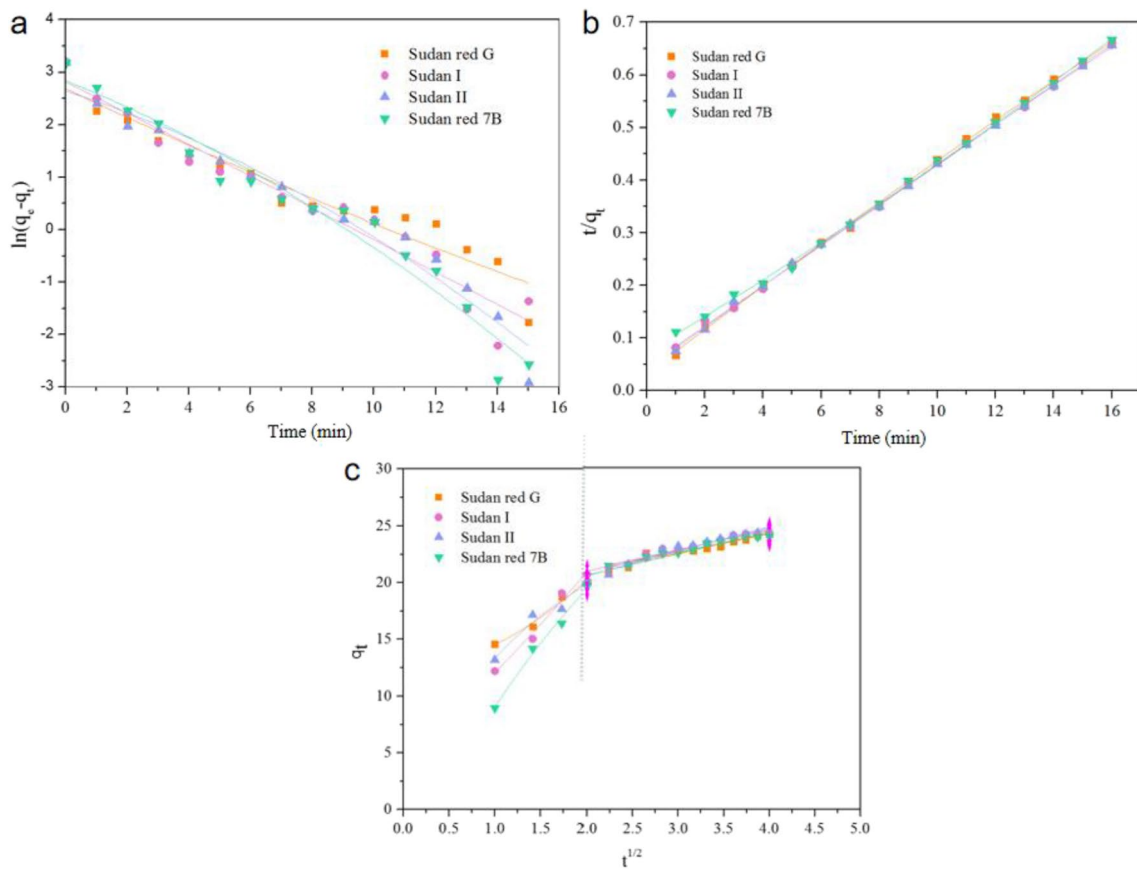**Fig. 6** The pseudofirst-level (**a**) and pseudosecond-level (**b**) models' linear curves and linear fitting curves for the intraparticle diffusion Model (**c**)

**Table 1** Kinetic parameters of dye adsorption by NSAC

| Dyestuff | $q_e$ (exp) | First-order kinetic model | | | Second-order kinetic model | | |
|---|---|---|---|---|---|---|---|
| | | $q_e$ (cal) | $k_1$ (min$^{-1}$) | $R^2$ | $q_e$ (cal) | $k_2$ (g mg$^{-1}$ min$^{-1}$) | $R^2$ |
| Sudan red G | 24.22 | 14.72 | 0.28 | 0.9201 | 23.75 | 0.0018 | 0.9993 |
| Sudan I | 24.32 | 16.71 | 0.30 | 0.9378 | 26.12 | 0.0015 | 0.9994 |
| Sudan II | 24.38 | 14.16 | 0.19 | 0.9558 | 25.02 | 0.0016 | 0.9995 |
| Sudan red 7B | 23.99 | 17.18 | 0.24 | 0.9555 | 30.13 | 0.0011 | 0.999 |

**Table 2** Parameters of the intraparticle diffusion model for dye adsorption by NSAC

| | kip1 (mg g$^{-1}$ min$^{-0.5}$) | $C_1$ | $R^2$ | kip 2 (mg g$^{-1}$ min$^{-0.5}$) | $C_2$ | $R^2$ |
|---|---|---|---|---|---|---|
| Sudan red G | 0.8227 | 12.0857 | 0.943 | 1.8632 | 16.875 | 0.9154 |
| Sudan I | 6.9961 | 4.4507 | 0.9461 | 1.8323 | 17.284 | 0.9568 |
| Sudan II | 12.5104 | 2.8769 | 0.8584 | 2.1481 | 16.2468 | 0.9429 |
| Sudan red 7B | 15.3311 | 4.6 | 0.9721 | 1.924 | 16.7302 | 0.9073 |

$$ln q_e = \frac{1}{n} ln C_e + ln K_F \qquad (8)$$

where $K_L$ (L $mg^{-1}$) is the Langmuir equilibrium adsorption constant related to affinity, $q_{max}$ (mg $g^{-1}$) is the maximum dye uptake under the operating conditions, and the values of $K_L$ and $q_{max}$ could be calculated by plotting a linear plot of $1/q_e$ against $1/C_e$ (Fig. 7a). Additionally, the separation factor $R_L$, which was calculated to determine the adsorption process information about the shape of the isotherm, could be obtained using Eq. (9). n and $K_F$ (L $mg^{-1}$) are the Freundlich adsorption constants and are related to the adsorption intensity and the adsorption capacity, respectively. A plot of ln $q_e$ against ln $C_e$ gives a line with an intercept of $K_F$ and a slope of 1/n (Fig. 7b).

$$R_L = \frac{1}{K_L C_0 + 1} \qquad (9)$$

The adsorption results at equilibrium obtained by the non-linear equations of the Langmuir and Freundlich isotherm models are displayed in Table 3 and were calculated from Fig. 7. The equilibrium data obtained in the Langmuir model had a higher $R^2$ value close to unity than that of the Freundlich isotherm model, which indicated that dye adsorption on NSAC is a homogeneous monolayer adsorption process

with uniform free energy change. Moreover, the maximum adsorption capacities of the four dyes on NSAC calculated according to the Langmuir adsorption model were 36.19, 35.64, 34.60 and 38.97 mg $g^{-1}$ for Sudan Red G, Sudan I, Sudan II and Sudan Red 7B, respectively, demonstrating that NSAC had excellent adsorption performance. The high intercept values correspond to the binding energy ($K_L$) of adsorption, which reflects the strong binding affinity of NSAC toward dye molecules. In addition, the determined values of $R_L$ were in the range from 0.0078 to 0.0231 with a low value, implying a favorable and irreversible process of adsorption.

## 3.6 Thermodynamic study of NSAC

The proper calculation of thermodynamic variables is an indispensable and important step in the study of the adsorption process. There are many theoretical methods for evaluating the thermodynamic variables involved in the adsorbate/adsorbent system, which usually rely on the application of reaction equilibrium constants. To understand the mechanism of the dye adsorption process on NSAC, the thermodynamics of the adsorption process were investigated by varying the temperature range from 30 to 50℃. Thermodynamic parameters viz.
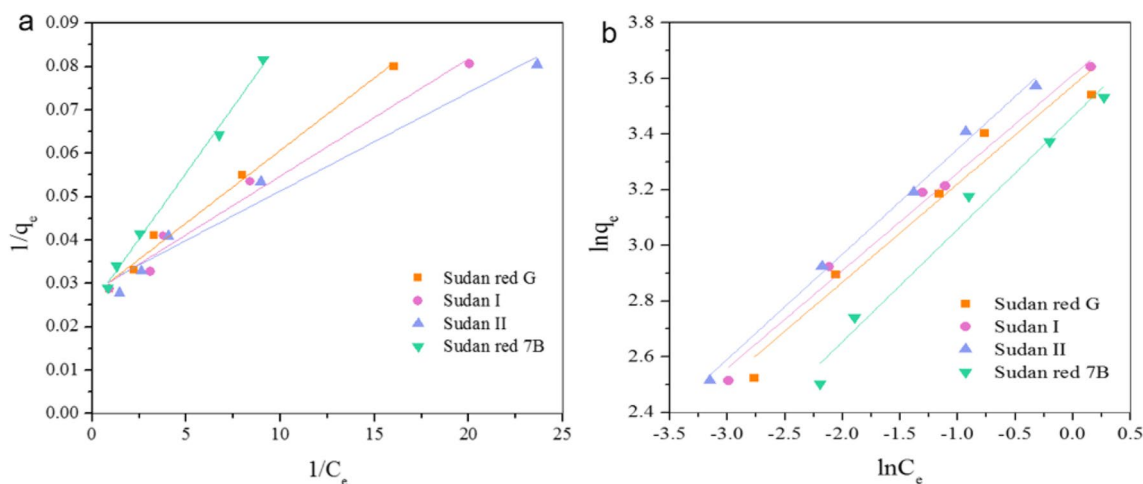


**Fig. 7** Langmuir isotherm Model (**a**) and Freundlich isotherm Model (**b**)

**Table 3** Parameters of the Langmuir and Freundlich adsorption isotherm models for dye adsorption by NSAC

|  | Langmuir isotherm model | | | Freundlich isotherm model | | |
|---|---|---|---|---|---|---|
|  | $q_m$ (mg $g^{-1}$) | $K_L$ (L $mg^{-1}$) | $R^2$ | $K_F$ (L $mg^{-1}$) | n | $R^2$ |
| Sudan red G | 36.1925 | 8.2725 | 0.9878 | 35.8162 | 2.8345 | 0.9467 |
| Sudan I | 35.6379 | 10.3926 | 0.9738 | 37.2034 | 2.8490 | 0.9861 |
| Sudan II | 34.6021 | 12.7313 | 0.9609 | 41.6250 | 2.6483 | 0.9942 |
| Sudan red 7B | 38.9712 | 4.2204 | 0.9940 | 32.0469 | 2.4740 | 0.9727 |

The equilibrium constant value ($K_0$), standard Gibbs free energy ($\Delta G^0$), enthalpy change ($\Delta H^0$) and entropy change ($\Delta S^0$) could provide useful information about the internal energy changes related to the adsorption process, which are determined from the best fitting isotherm using Eq. (10) and Eq. (11).

$$\Delta G^0 = -RT \ \ln \ K_0 \tag{10}$$

$$\ln \ K_0 = \Delta S^0/R - \Delta H^0/RT \tag{11}$$

where $K_0$ is the equilibrium constant, T and R are the absolute temperature (K) and the universal gas constant (8.314 J mol$^{-1}$·K), respectively. Both $\Delta H0$ and $\Delta S^0$ could be calculated from the plot of $\ln K_0$ against 1/T.

The results illustrated in Table 4 show that the adsorption equilibrium constant values of the four dyes increased with increasing temperature, indicating that the temperature promoted the adsorption of dyes. The calculated positive $\Delta H^0$ value of dye adsorption indicated that the adsorption process of dye molecules onto NSAC had endothermic properties, explaining that the adsorption capacity increased with increasing temperature. In addition, $\Delta S^0$ was also positive, which meant that the endothermic interaction between the dye and the adsorbent increased the randomness of the adsorption of the dye on the NSAC. Finally, the negative value of $\Delta G^0$ obtained at higher temperatures indicated that the dye adsorption removal process performed at different temperatures is very feasible, more spontaneous, and extremely beneficial at higher temperatures. Moreover, the fact that $\Delta G^0$ values decreased with increasing adsorption temperature also explains the endothermic nature of dye adsorption on NSAC.

## 3.7 Regeneration and real sample studies

For activated carbon to be more economical, feasible and applicable, it should have a higher regeneration potential. Therefore, its reusability should be evaluated in practical applications. Usually, desorption experiments are carried out to investigate the feasibility of activated carbon reuse, and the adsorbate is desorbed from the adsorbent with the help of agitation and chemical eluent in the desorption process. Figure 8 shows the effect of the regeneration cycle of NSAC using ethanol as the eluent on the dye adsorption efficiency under optimized conditions. After 3 cycles of reuse, the relative recoveries of the prepared NSAC decreased from 96.96 to 90.34% for Sudan Red G, 97.83% to 82.49% for Sudan I, 97.1% to 72.29% for Sudan II and 94.03% to 68.24% for Sudan Red 7B, which proved that NSAC was a good adsorbent with excellent reusability and stability. To evaluate the practicability and versatility of the adsorbent, NSAC was used in dye solution adsorption experiments with chrysanthemum and egg samples as the matrix. The relative recoveries of chrysanthemum and egg ranged from 88.57% to 100.14% and 86.27% to 110.81%, respectively. Consequently, NSAC was successfully applied to remove dyes from chrysanthemum and egg samples.

## 3.8 Comparison of other activated carbons

To evaluate the adsorption capacity of activated carbon synthesized from Nelumbinis stamen as a precursor for dyes, it was compared with the adsorption performance of activated carbon synthesized from different food wastes for different dyes reported in the literature, and the results are shown in Table 5. As shown in the table, various food wastes were applied as precursors for the preparation of activated
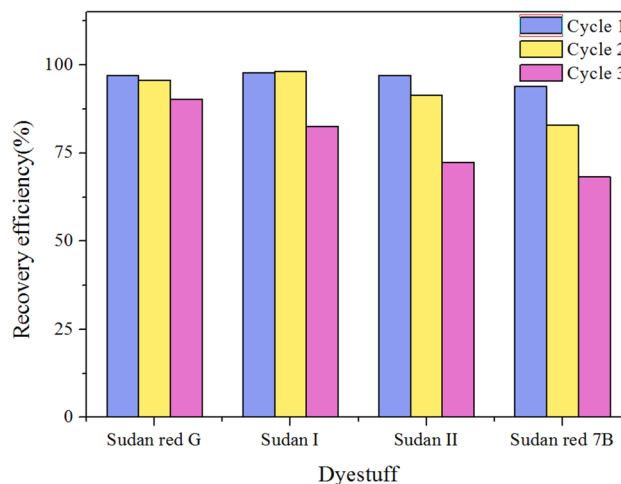
**Table 4** Thermodynamic parameters of NSAC-adsorbed dyes

| Dyestuff | Temperature (K) | $\ln K_0$ | $\Delta G^0$ (kJ mol$^{-1}$) | $\Delta H^0$ (kJ mol$^{-1}$) | $\Delta S^0$ (kJ mol$^{-1}$ K$^{-1}$) |
|---|---|---|---|---|---|
| Sudan red G | 303 | 3.2642 | -8.223 | 42.910 | 172.13 |
| | 313 | 4.0232 | -10.470 | | |
| | 323 | 4.7186 | -12.671 | | |
| Sudan I | 303 | 3.8067 | -9.590 | 28.429 | 126.02 |
| | 313 | 4.3708 | -11.374 | | |
| | 323 | 4.5011 | -12.087 | | |
| Sudan II | 303 | 3.6605 | -9.221 | 37.873 | 156.04 |
| | 313 | 4.3649 | -11.358 | | |
| | 323 | 4.5866 | -12.317 | | |
| Sudan red 7B | 303 | 2.8767 | -7.247 | 25.867 | 109.41 |
| | 313 | 3.2513 | -8.461 | | |
| | 323 | 3.5115 | -9.430 | | |



**Fig. 8** The effect of the regeneration cycle of NSAC

**Table 5** Comparison of the Sudan dye maximum adsorption capacities ($q_m$) of NSAC with other activated carbons derived from food waste

| The precursor of AC | Pollutant | Activation | $q_m$ (mg g$^{-1}$) | Reference |
|---|---|---|---|---|
| Cherry tree | Cationic red 14 dye | 85% $H_3PO_4$, 24 h | 348.61 | [34] |
| Macadamia husk | Malachite green | 85% $H_3PO_4$, 1 h | ~130 | [35] |
| Durian seeds, Rambutan peels | Methylene blue | $H_3PO_4$, 24 h | 118.5 | [36] |
| Argan waste | Methyl orange and Methylene blue | $H_3PO_4$ | 31–70 | [37] |
| Sugarcane bagasse, Spent-coffee ground, and Orange peel | Methyl orange and Methylene blue | concentrated $H_3PO_4$ | 10–75 | [38] |
| Argan nutshell | Rhodamine B | $Na_2CO_3$, 24 h | 35.9 | [39] |
| Onion waste | Crystal violet | 3 M KOH overnight | 18.6 | [40] |
| Nelumbinis stamen | Sudan Red G, Sudan I, Sudan II, and Sudan Red 7B | 60% $H_3PO_4$, 2 h | 34.60–38.97 | This study |

carbon, such as cherry tree, macadamia husk, durian seeds, Rambutan peels, and argan nutshell. The prepared activated carbon was employed for the adsorption of different dyes, such as cationic red 14 dye, malachite green, methyl orange, methylene blue, and rhodamine B. In contrast, this work is the first time that Nelumbinis stamen has been employed as a precursor to activated carbon, and the activation time is relatively short. Meanwhile, this is also the first time that activated carbon has been used for the adsorption of Sudanese dyes. The results demonstrated that NSAC was quite effective in the adsorption of Sudan Red G, Sudan I, Sudan II and Sudan Red 7B with maximum adsorption capacities of 36.19, 35.64, 34.60 and 38.97 mg g$^{-1}$, respectively, indicating that Nelumbinis stamen could be used as one of the most promising activated carbon precursors for the adsorption of Sudan dyes.

## 4 Conclusion

In this work, a novel activated carbon prepared by Nelumbinis stamen was successfully applied as an efficient and economical adsorbent, which possessed a large specific surface area (732.98 m$^2$ g$^{-1}$) and showed high adsorption ability for Sudan dye removal from plants and eggs. Together with kinetic and thermodynamic studies, dye adsorption on NSAC in an aqueous solution was performed by studying the influence of adsorbent dosage, adsorption temperature, and pH. The adsorption process reached adsorption equilibrium within 16 min for the studies performed in this paper. The kinetic and equilibrium data showed that dye adsorption onto the NSAC could be described by pseudosecond-order and Langmuir models, respectively. Additionally, the calculated thermodynamic parameters revealed that dye adsorption onto the NSAC was endothermic, and the spontaneous nature of the adsorption process was supported by the negative values of $\Delta G^0$.

After 3 recycling cycles, the removal efficiency of Sudan dyes was still above 68%. In general, Nelumbinis stamen is a promising activated carbon precursor with great potential for application in the treatment of wastewater containing Sudan dyes and even other types of wastewater.

## Declarations

## References

1. Wen Z, Wang Y, De-Clercq D (2016) What is the true value of food waste? a case study of technology integration in urban food waste treatment in suzhou city, China. J Clean Prod 118:88–96
2. Badgett A, Milbrandt A (2021) Food waste disposal and utilization in the United States: A spatial cost benefit analysis. J Clean Prod 314:128057
3. Esparza I, Jimenez-Moreno N, Bimbela F (2020) Fruit and vegetable waste management: Conventional and emerging approaches. J Environ Manage 265:110510
4. Zhang S, Shi YQ, Tai J et al (2022) Mapping the impact of a large municipal waste disposal area on surface water: 1993–2017, case of Laogang, Shanghai. Waste Manage 148:50–60

5. Chu ZJ, Fan XH, Wang W et al (2019) Quantitative evaluation of heavy metals' pollution hazards and estimation of heavy metals' environmental costs in leachate during food waste composting. Waste Manage 84:119–128

6. Hui SN, Kee PE, Yim HS et al (2020) Recent advances on the sustainable approaches for conversion and reutilization of food wastes to valuable bioproducts. Bioresource Technol 302:122889

7. Nguyen TN, Le PA, Phung VBT (2022) Facile green synthesis of carbon quantum dots and biomass-derived activated carbon from banana peels: synthesis and investigation. Biomass Convers Bior 12:2407–2416

8. Wang Y, Wang SL, Xie T et al (2020) Activated carbon derived from waste tangerine seed for the high-performance adsorption of carbamate pesticides from water and plant. Bioresource Technol 316:123929

9. Zhen XT, Yu YL, Shi MZ et al (2022) Activated carbon derived from hawthorn kernel waste for rapid adsorption of fungicides. Surf Interfaces 28:101700

10. Karaoğlu K, Özçifçi Z, Çalışkan M et al (2022) Catalytic activity of palladium doped activated carbon from waste coffee on some environmental pollutants. Mater Chem Phys 282:125857

11. Pang XN, Sellaoui L, Francoc D et al (2019) Adsorption of crystal violet on biomasses from pecan nutshell, para chestnut husk, araucaria bark and palm cactus: Experimental study and theoretical modeling via monolayer and double layer statistical physics models. Chem Eng J 378:122101

12. Wang JL, Wang SZ (2019) Preparation, modification and environmental application of biochar: A Review. J Clean Prod 227:1002–1022

13. Mbarki F, Selmi T, Kesraoui A et al (2022) Low-cost activated carbon preparation from Corn stigmata fibers chemically activated using $H_3PO_4$, $ZnCl_2$ and KOH: Study of methylene blue adsorption, stochastic isotherm and fractal kinetic. Ind Crop Prod 178:114546

14. Bouchelkia N, Tahraoui H, Amrane A et al (2023) Jujube stones based highly efficient activated carbon for methylene blue adsorption: Kinetics and isotherms modeling, thermodynamics and mechanism study, optimization via response surface methodology and machine learning approaches. Process Saf Environ 170:513–535

15. Mohan D, Sarswat A, Ok YS et al (2014) Organic and inorganic contaminants removal from water with biochar, a renewable, low cost and sustainable adsorbent – A critical review. Bioresource Technol 160:191–202

16. Zeghioud H, Fryda L, Djelal H (2022) A comprehensive review of biochar in removal of organic pollutants from wastewater: Characterization, toxicity, activation/functionalization and influencing treatment factors. J Water Process Eng 47:102801

17. Dinh VP, Nguyen DK, Luu TT et al (2022) Adsorption of Pb (II) from aqueous solution by pomelo fruit peel-derived biochar. Mater Chem Phys 285:126105

18. Zein R, Suhaili R, Earnestly F et al (2010) Removal of Pb (II), Cd (II) and Co (II) from aqueous solution using *Garcinia mangostana* L. fruit shell. J Hazard Mater 181:52–56

19. Doke KM, Khan EM (2017) Equilibrium, kinetic and diffusion mechanism of Cr(VI) adsorption onto activated carbon derived from wood apple shell. Arab J Chem 10:252–260

20. Imran M, Natasha MB et al (2022) Potential of nanocomposites of zero valent copper and magnetite with Eleocharis dulcis biochar for packed column and batch scale removal of Congo red dye. Environ Pollut 305:119291

21. Wozniak MM, Witkowski B, Ganeczko M et al (2021) Textile dyeing in Medieval Sudan evidenced by HPLC-MS analyses: Material traces of a disappeared activity. J Archaeol Sci 38:103098

22. Shen Y, Mao SD, Chen F et al (2022) Electrochemical detection of Sudan red series azo dyes: Bibliometrics based analysis. Food Chem Toxicol 163:112960

23. Reile CG, Rodríguez MS, Fernandes DDS et al (2020) Qualitative and quantitative analysis based on digital images to determine the adulteration of ketchup samples with Sudan I dye. Food Chem 328:127101

24. Moreno-González D, Jáč P, Švec F et al (2020) Determination of Sudan dyes in chili products by micellar electrokinetic chromatography-MS/MS using a volatile surfactant. Food Chem 310:125963

25. Ozak SS, Yılmaz Y (2020) Ultrasound-assisted hydrophobic deep eutectic solvent based solid-liquid microextraction of Sudan dyes in spice samples. Spectrochim Acta A 236:118353

26. Liu JS, Guo YJ, Zhang J et al (2014) Systematic chemical analysis of flavonoids in the Nelumbinis stamen. Phytomedicine 21:1753–1758

27. Chen XF, Wan SY, Ding JH et al (2021) Oxygen-sulfur-phosphorus co-doped activated carbon derived from lotus stamens for high-performance supercapacitors. Chinese J Anal Chem 49:75–81

28. Xue HJ, Gao X, Seliem MK et al (2023) Efficient adsorption of anionic azo dyes on porous heterostructured MXene/ biomass activated carbon composites: Experiments, characterization, and theoretical analysis via advanced statistical physics models. Chem Eng J 451:138735

29. Zhu XY, Lin HM, Chen X et al (2011) Mechanochemical-assisted extraction and antioxidant activities of kaempferol glycosides from Camellia oleifera Abel. Meal J Agric Food Chem 59:3986–3993

30. Dhelipan M, Arunchander A, Sahu AK et al (2017) Activated carbon from orange peels as supercapacitor electrode and catalyst support for oxygen reduction reaction in proton exchange membrane fuel cell. J Saudi Chem Soc 21:487–494

31. Wang XM, Xu Q, Zhang L et al (2023) Adsorption of methylene blue and Congo red from aqueous solution on 3D MXene/carbon foam hybrid aerogels: A study by experimental and statistical physics modeling. J Environ Chem Eng 11:109206

32. Song LX, Yang ZK, Teng Y et al (2013) Nickel oxide nanoflowers: formation, structure, magnetic property and adsorptive performance towards organic dyes and heavy metal ions. J Mater Chem A 1:8731–8736

33. Wang T, Yang W, Song T et al (2015) Cu-doped Fe3O4 magnetic adsorbent for arsenic: synthesis, property, and sorption application. RSC Adv 5:50011–50018

34. Roya A, Mohammadi F, Moharrami A et al (2023) Synthesis of activated carbon from cherry tree waste and its application in removing cationic red 14 dye from aqueous environments. Appl Water Sci 13:90

35 Wattanasiriwech S, Naradisorn M, Wattanasiriwech D (2022) Adsorption performance of macadamia husk-activated carbon from a household pyrolysis kiln. Green Mater. https://doi.org/10.1680/jgrma.22.00096

36. Farki NNANLT, Abdulhameed AS, Surip SN et al (2023) Tropical fruit wastes including durian seeds and rambutan peels as a precursor for producing activated carbon using $H_3PO_4$-assisted microwave method: RSM-BBD optimization and mechanism for methylene blue dye adsorption. Int J Phytoremediat. https://doi.org/10.1080/15226514.2023.2175780

37. Ouedrhiri A, Ennabely M, Lghazi Y et al (2023) Adsorption of anionic and cationic dyes in aqueous solution by a sustainable and low-cost activated carbon based on argan solid waste treated with $H_3PO_4$. Environ Sci Pollut R. https://doi.org/10.1007/s11356-023-26550-z

38. Martínez RJ, Vela-Carrillo AZ, Godínez LA et al (2023) Competitive adsorption of anionic and cationic molecules on three activated carbons derived from agroindustrial waste. Biomass Bioenerg 168:106660

39. Ouardi YE, Aissouq AE, Chennah A et al (2022) Synthesis, characterization, and DFT investigation of rhodamine B dye removal by activated carbon produced from argan nutshell. Biomass Conversion Biorefner. https://doi.org/10.1007/s13399-022-03706-4

40. Bibi F, Sattar A, Hussain S et al (2023) Tailoring the sorption properties of crystal violet by activated carbon extracted from waste onion. Chem Pap. https://doi.org/10.1007/s11696-023-02756-w